Astronomische
Nachrichten

The hyperluminous X-ray source population

A. D. A. MacKenzie[1] | **T. P. Roberts[1]** | **D. J. Walton[2,3]**

[1]Centre for Extragalactic Astronomy & Department of Physics, Durham University, Durham, UK

[2]School of Physics, Astronomy and Mathematics, University of Hertfordshire, Hertfordshire, UK

[3]Institute of Astronomy, University of Cambridge, Cambridge, UK

Correspondence
A. D. A. MacKenzie, Centre for Extragalactic Astronomy & Department of Physics, Durham University, Durham, UK.
Email:
angus.d.mackenzie@durham.ac.uk

Present Address
Department of Physics, Durham, UK

Funding information
Science and Technology Facilities Council, Grant/Award Number: ST/000244/1

Abstract
We have recently published a catalog of 1843 candidate ultraluminous X-ray sources (ULXs). This is the largest catalog of ULXs to date and was built by cross-correlating recent serendipitous source catalogs from the *XMM-Newton*, *Swift*, and *Chandra* observatories with a large sample of galaxies, primarily from HyperLEDA. The catalog contains 71 hyperluminous X-ray source (HLX) candidates, the most extreme members of the ULX population with luminosities above 10^{41} erg s^{-1}. These sources are often considered the best candidates for intermediate-mass black hole (IMBH) accretors and include the archetypal IMBH candidate ESO 243–49 HLX-1. However, the most luminous of the known pulsating ULXs, NGC 5907 ULX1, is also an HLX at its brightest. We demonstrate that these two objects occupy distinct areas of the hardness-intensity parameter space, and use this to contextualize the results from a pilot study of three data-rich examples of the 42 HLXs we select as the best candidates based on their multi-wavelength counterparts and X-ray data quality. We briefly discuss the implications of this work.

KEYWORD
X-rays: binaries

1 | INTRODUCTION

Ultraluminous X-ray sources (ULXs) are point-like objects found in external galaxies (Kaaret et al. 2017). They are characterized by an X-ray luminosity, $L_{X,\text{peak}} \geq 10^{39}$ erg s^{-1} but are located outside the nuclei of galaxies, removing contributions to the class from active galactic nuclei (AGN). It is now thought that accreting binaries exceeding their Eddington limit dominate the ULX population. This has been confirmed by the discovery of pulsating ULXs (PULXs) that must contain neutron stars (NSs) and which appear to shine at $\gtrsim 10\times L_{\text{Edd}}$. These were

discovered by the detection of coherent pulsations from known ULXs: currently-identified PULXs include M82 X-2 (Bachetti et al. 2014), NGC 7793 P13 (Fürst et al. 2016; Israel et al. 2017), NGC 5907 ULX1 (Israel et al. 2017), NGC 300 ULX-1 (Carpano et al. 2018), NGC 1313 X-2 (Sathyaprakash et al. 2019) and M51 ULX-7 (Rodríguez Castillo et al. 2020). However, the ULX population appears to remain heterogeneous to some degree, as a limited number of strong intermediate-mass black hole (IMBH) candidates, for example, ESO 243–49 HLX-1 (Farrell et al. 2009), M82 X-1 (Feng & Kaaret 2010; Pasham et al. 2014) and NGC 2276–3c (Mezcua et al. 2015) are counted among the ULX class.

Black hole accretion under the X-ray microscope—ESAC, Madrid.

TABLE 1 Examples of ultraluminous X-ray (ULX) catalogues.

Year	Authors	Mission	ULXs	Hosts
2000	Roberts & Warwick	*ROSAT*	28	19
2004	Swartz et al.	*Chandra*	154	82
2011	Walton et al.	*XMM-Newton*	470	238
2019	Earnshaw et al.	*XMM-Newton*	384	241
2020	Kovlakas et al.	*Chandra*	629	238[a]
2022	Walton et al.	Multi[b]	1843	951

[a] Sample limited to within 40 Mpc.
[b] *Swift*, *XMM-Newton* and *Chandra*.

Both PULXs and good IMBH candidates are rare. One way to attempt to increase their numbers is to widen the pool of known ULXs; we do this by constructing new ULX catalogs. They require two major inputs, an X-ray source catalog, and a catalog of galaxies. The sky area subtended by the galaxy, defined here by its *D*25 ellipse, is used to match a given X-ray source to a host galaxy, then the best available galaxy distance determines the X-ray source luminosity. Examples of a handful of ULX catalogs can be found in Table 1. From such catalogs, we can derive a series of sub-populations for further analysis, for example, Sutton et al. (2012) worked on a sample of the most luminous detected ULXs from Walton et al. (2011), and Song et al. (2020) began their search for transient ULXs from the *XMM-Newton* catalog of Earnshaw et al. (2019). The latter was motivated by the potential link between PULXs and strong long-term variability, as this may be a direct consequence of the propeller effect in an accreting neutron star (Earnshaw et al. 2018; Tsygankov et al. 2016).

2 | A MULTI-MISSION CATALOGUE OF ULXS

Walton et al. (2022; hereafter W22) is a recently published catalog of ULXs compiled by searching for ULX candidates across three separate missions: *XMM-Newton*, *Chandra*, and *Swift*. X-ray data were taken from a recent version of each mission's serendipitous source catalog, these being 4XMM-DR10 (Webb et al. 2020), CSC2.0 (Evans et al. 2020) and 2SXPS (Evans et al. 2020) respectively, and matched against a catalog of galaxies primarily derived from the HyperLEDA archive (Makarov et al. 2014). Each mission's X-ray data were extracted at the observation level, to retain information on the sources' long-term behavior. This allowed for the incorporation of ULX transients into the catalog, objects which may be below the ULX threshold for some fraction of their observations but have been observed at peak luminosities $L_{X,peak} \geq 10^{39}$ erg s^{-1}. The

simultaneous use of data from three different X-ray missions introduced non-uniformity to the ULX catalog, as each mission carries instruments with different sensitivities across (largely overlapping) different energy ranges. Data from each of the three X-ray missions were used to generate separate ULX samples and then unique ULXs were identified across the different instruments by positional cross-matches. All the individual, observation-level information from each instrument was retained to permit transient searches.

The aim was to compile the largest raw sample of ULXs to date and the result is a published meta-catalog of 1843 candidate ULXs,[1] including 689 cataloged as such for the first time, with an estimated ~20% residual contamination.[2] This catalog can then be filtered to look for interesting sub-populations. One such population is the hyperluminous X-ray sources (HLXs), the most luminous of all accreting binaries that are characterized by $L_{X,peak} \geq 10^{41}$ erg s^{-1}. We detect only 71 HLX candidates in the catalog of 1843 ULXs, roughly one for every 27 sources, despite their increased luminosity making them detectable over much larger volumes of space than typical ULXs and so emphasizing the rarity of this class. However, the estimated contamination fraction is likely higher for the HLXs than the full catalog (cf. Sutton et al. 2012), with several previous good HLX candidates having been revealed as background QSOs, for example, an object associated with IC 4320 was shown to be a $z \sim 2.84$ QSO by Sutton et al. (2015).

3 | HLX SAMPLE CLEANING

The increased likelihood of background contamination for the HLX regime means we must be very careful when selecting objects for further study. Hence, we visually inspect each of the 71 candidates using publicly-available X-ray, optical and infrared images. A flowchart demonstrating our general process is shown in Figure 1. We first search for any optical counterpart in the available SDSS9, DSS, or PanSTARRS/DR1 data. At the sensitivities of these surveys and given the distances to the HLX host galaxies we would not expect to detect the accretion discs or individual stellar counterparts in the optical, indeed any detected counterpart would have an X-ray/optical flux ratio consistent with an AGN. So, in the case where an optical counterpart is identified within the

---

[1] The catalogue will eventually be available via the VizieR service, but can also be downloaded from the following link: https://dwalton354.wixsite.com/djwalton/ulxcatCatalogue Access

[2] This estimate is based on the sensitivity maps for each contributing observation and the empirically determined forms of the $\log N - \log S$ curves (see W22 for more details)
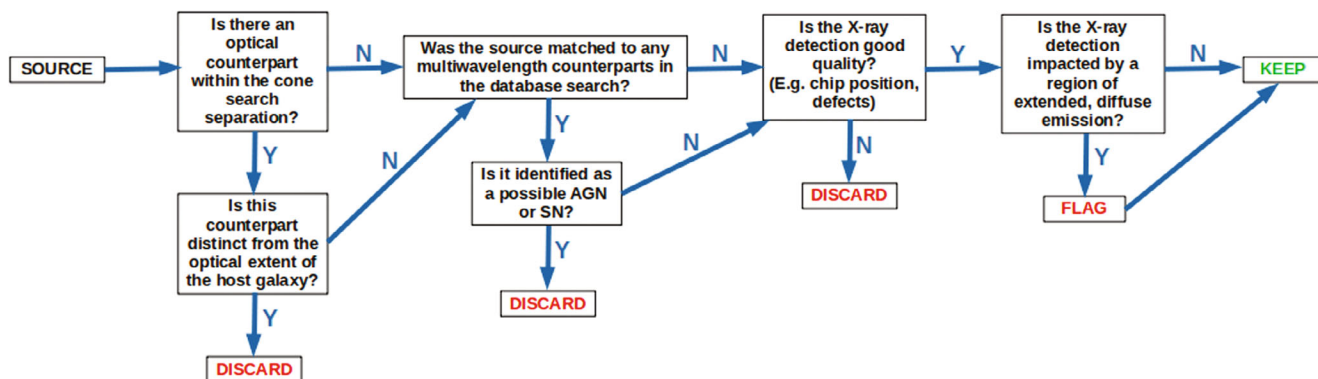
FIGURE 1 Flow diagram depicting the process by which good hyperluminous X-ray source (HLX) candidates were selected.

standard positional matching radius for each mission (see W22) and is distinct from the structure within the host galaxy, we define that source as a poor HLX candidate and exclude it from further analysis. Similarly, any object with a multi-wavelength counterpart consistent with an AGN (or a recent SN, if not already excluded in W22) is excluded. We also check the quality of the X-ray detection, using both the individual observation which secures it in our HLX sample (the highest peak luminosity) and other observations of the source position if necessary (e.g., to identify spurious detections due to detector artifacts). Again, if the detection appears questionable, the object is excluded from further analysis. Finally, any further detection in which a source is embedded in the diffuse X-ray emission of the host galaxy or a galaxy cluster is flagged as having potentially compromised X-ray emission, but in this case, it remains among the HLX candidate sample subject to further analysis.

4 | A SAMPLE OF PROMISING HLX CANDIDATES

After the cleaning process detailed in Section 3, we are left with a sample of 42 good HLX candidates. For each of these sources, we extracted and analyzed all available X-ray data across the three missions used in our catalog. Spectra were extracted for any individual observations (or *Swift* data stacks) with sufficient counts, and best fits were produced for simple spectral models. Where insufficient counts were present, hardness ratios were used to provide approximate spectral shapes, or (in a few cases) standard spectral forms for ULXs were assumed (Gladstone et al. 2009). This information (alongside galaxy distances adopted in W22) was then used to convert count rates from each observation to luminosities, which were used to determine long-term light curves for each HLX. Count rates above and below 2 keV were also determined for each observation; again using the spectral information

any *XMM-Newton* or *Chandra* count rates were converted to their *Swift* equivalents, and so we were able to also produce hardness-luminosity (equivalent to color-intensity) plots for each HLX.[3] Three examples of these data are shown in Figures 2–4.

In order to better understand what the data—especially the hardness-luminosity plots—reveal, we place our HLXs in context by comparison to the properties of two well-studied HLXs: the confirmed PULX, NGC 5907 ULX1, and the strong IMBH candidate, ESO 243–49 HLX-1. Some properties of each source are summarized in Table 2. Clearly, the two archetypes occupy distinct areas of parameter space, making them useful as comparators, although it is worth noting that ESO 243–49 HLX1 has been observed during lower luminosity, spectrally hard phases in the extremes of the data, beyond the 75% encapsulation contour.

This comparison permits us to directly ask questions such as: do the PULX and the IMBH candidate represent archetypes of the wider HLX population? Do our HLX candidates resemble and exhibit the behavior of only one of these two objects? Is there a split among the population between each archetype? Or do our sources occupy the center of the parameter space, with a given source exhibiting properties consistent with both ESO 243–49 HLX-1 and NGC 5907 ULX1 in different observations? For this work, we selected three HLXs to pilot the analysis, on the basis of good coverage in all three missions we consider. The data for these objects are displayed in Figures 2–4, with the left-hand panel in each case also showing the areas of hardness-luminosity parameter space occupied by the two comparator archetypes.

Figure 2 shows the first of our pilot HLX candidates, which is associated with the galaxy IC 1633. Its long-term light curve shows its luminosity was initially below 10^{41} erg s^{-1}, but it increased such that the source

---

[3]The hardness ratio was calculated as (hard−soft)/(hard+soft), with appropriate errors.
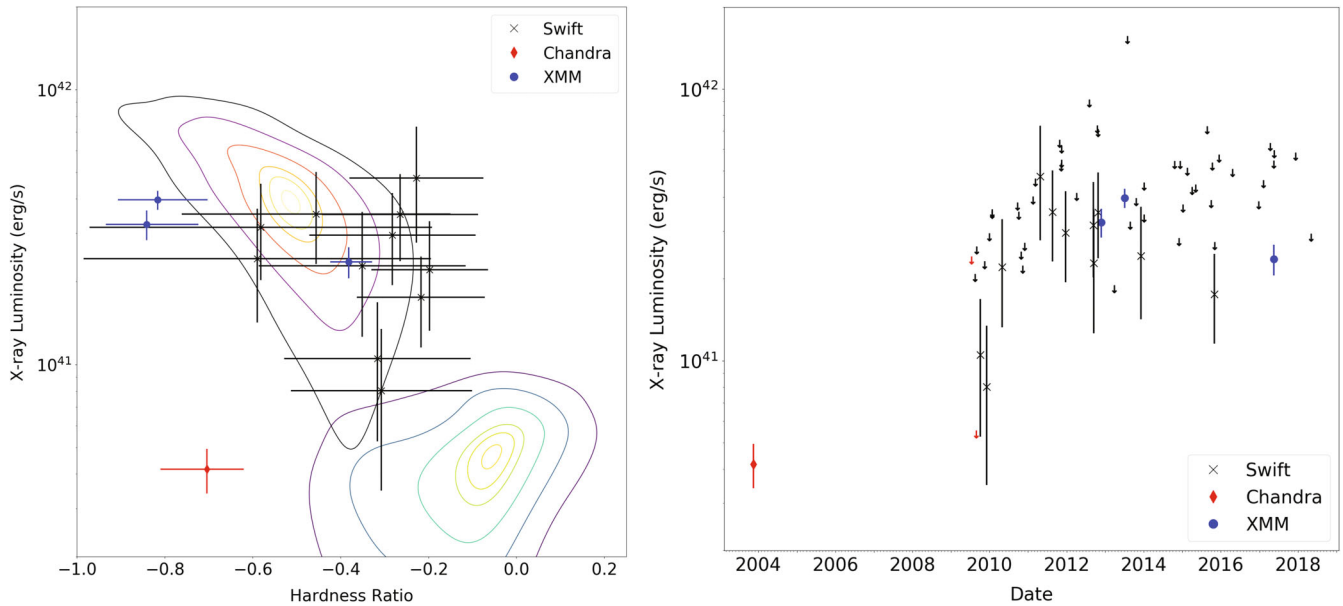
FIGURE 2 Data for an hyperluminous X-ray source (HLX) candidate in IC 1633. The HLX is at a distance of 92.9 Mpc. (*Left*) Hardness-luminosity diagram with data points overlaid as per the legend. The contours depict the parameter space occupied by the multitude of *Swift* observations for either archetype, with the contours plotted at 1%, 5%, 10%, 25%, 50%, and 75% of observations encapsulated by the contours. ESO 243–49 HLX-1 is represented by the redder color scheme (top left of the figure), with NGC 5907 ULX1 represented by the bluer colors (bottom right). (*right*) Long-term light curve, with data points (including 3σ upper limits) again as per the legend.
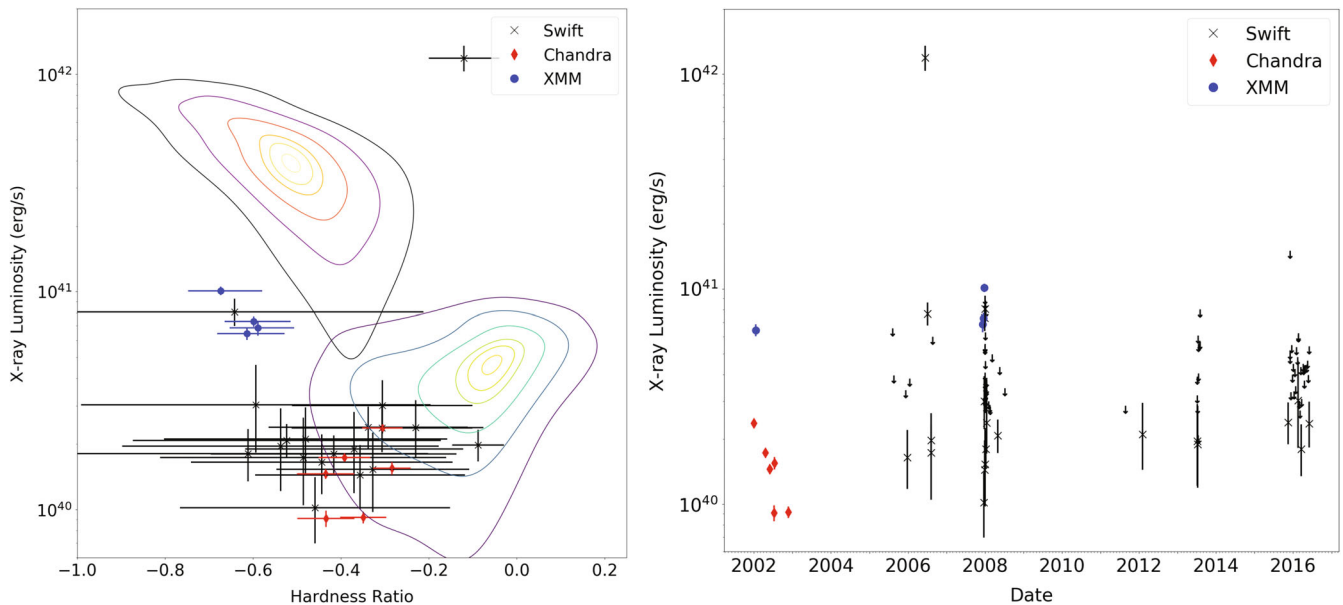
FIGURE 3 As per Figure 2, for an hyperluminous X-ray source (HLX) candidate in NGC 4038 at 22.1 Mpc.

entered the HLX regime in October 2009 and remained in it thereafter. With the exception of an early *Chandra* detection, this object appears to occupy very similar hardness-luminosity parameter space to ESO 243–49 HLX-1. However, this object is flagged as it lies in a galaxy with a high diffuse X-ray emission content; it is unclear without further analysis whether the softness

and luminosity of the source are intrinsic, or a result of contamination of the larger *Swift* and *XMM-Newton* apertures by the diffuse emission. This will be examined in future work.

Our second pilot HLX candidate is in NGC 4038 (one of the Antennae galaxies). We display its data in Figure 3. Its long-term light curve demonstrates that it largely emits at
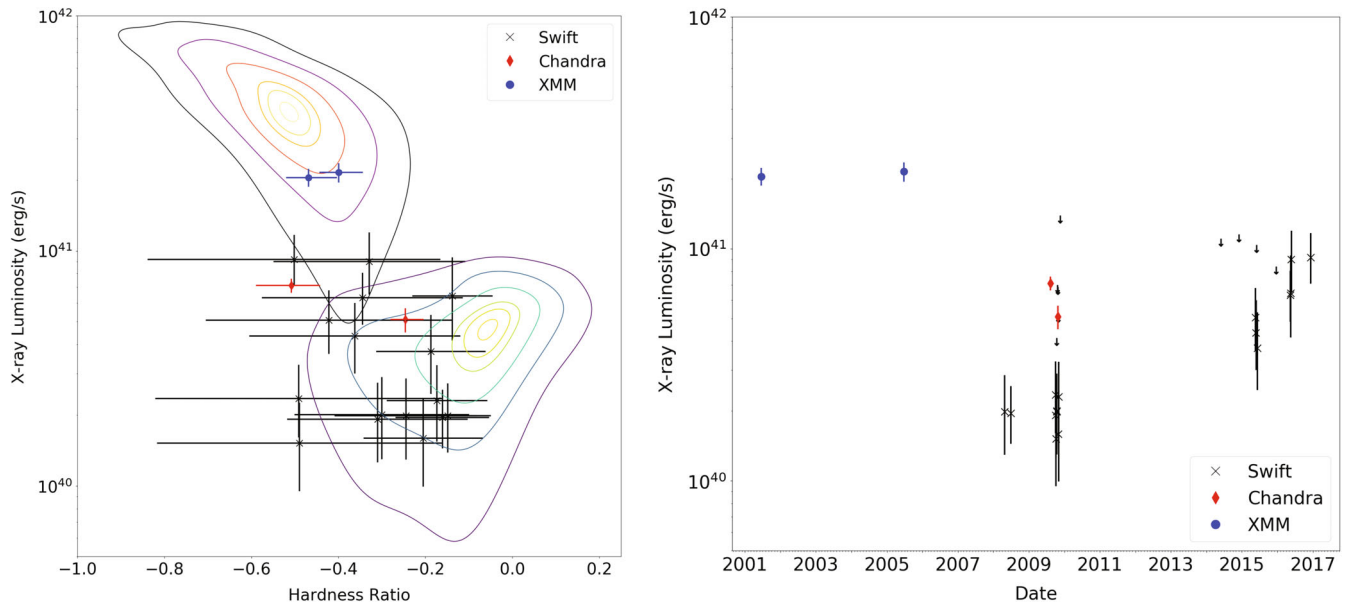
FIGURE 4   As per Figure 2, for an hyperluminous X-ray source (HLX) candidate in NGC 7479 at 36.8 Mpc.

TABLE 2   Hyperluminous X-ray source (HLX) archetypes: general properties.

NGC 5907 ULX1[a]	ESO 243–49 HLX-1[b]
Pulsations detected	Sub-Eddington accretion states at a high L_X
⇒ neutron star accretor	⇒ strong IMBH candidate
Transient; a 78-day period when "on"	Initial ∼ yearly outbursts with $L_{X,peak}$ ∼10^{42} erg s^{-1}
Peak L_X > 500× its Eddington limit	Outburst period lengthened and the source faded over ∼ a decade

Note: For further info, see (for example):
[a] Fürst et al. (2017), Israel, Belfiore, et al. (2017), Walton et al. (2015).
[b] Farrell et al. (2009), Lin et al. (2020), Webb et al. (2012).

luminosities well below the HLX regime. Indeed, the single extreme luminosity ($L_X \sim 10^{42}$ erg s^{-1}) data point has subsequently been identified as spurious. Given that the Antennae are a source- and diffuse emission-rich system, the brighter (and softer) *XMM-Newton* data points also merit further investigation as to whether they are the result of source confusion, particularly given the much lower contemporaneous *Chandra* luminosities early in the light curve. The lower luminosity points appear moderately hard and overlap somewhat with the NGC 5907 ULX-1 contours.

The HLX in NGC 7479 (Figure 4) appears most like NGC 5907 ULX1 in the hardness-luminosity plot and typically emits below HLX luminosities. We note that at least some of the hardness of NGC 5907 ULX1 comes from it being embedded in an edge-on galaxy disc, so it may be

unrealistic to expect a source in a face-on system such as NGC 7479 to be quite as spectrally hard. However, in the two earliest (*XMM-Newton*) observations, this object is clearly in the HLX regime, and it lies within the 50% contour for ESO 243–49 HLX-1. This is unlikely to be due to contamination, as this object is relatively isolated. This object is therefore very interesting in the range of luminosity and spectral hardness it displays, which overlaps both archetypes. Its most recent observations showed it to be increasing in luminosity and re-entering the HLX regime.

5 | CONCLUSIONS

We have derived a large sample of HLXs from the W22 ULX meta-catalog, numbering more than 40 objects after the removal of poor candidates. We have presented a pilot study of three data-rich objects, including a comparison of two possible archetypes for this regime, the PULX NGC 5907 ULX1, and the IMBH candidate ESO 243–49 HLX-1. This pilot study leaves us with multiple questions, on the quality of the data for two of the objects (and by extension whether potential confusion problems may be rife within the sample), and on the physical basis of the range of behavior for the third. These will be examined further, alongside the remaining sample, in future work (MacKenzie et al. in preparation).

With reference to the questions in Section 4, three sources are insufficient to address them fully. We must look at the complete sample to begin answering them. However, the NGC 7479 object clearly occupies the

parameter space of both archetypes, so more work is necessary.

ORCID

A. D. A. MacKenzie https://orcid.org/0000-0002-5268-5609

REFERENCES

Bachetti, M., Harrison, F. A., Walton, D. J., et al. 2014, *Nature*, *514*(7521), 202.

Carpano, S., Haberl, F., Maitra, C., & Vasilopoulos, G. 2018, *MNRAS*, *476*(1), L45.

Earnshaw, H. P., Roberts, T. P., Middleton, M. J., Walton, D. J., & Mateos, S. 2019, *MNRAS*, *483*(4), 5554.

Earnshaw, H. P., Roberts, T. P., & Sathyaprakash, R. 2018, *MNRAS*, *476*(3), 4272.

Evans, I. N., Primini, F. A., Miller, J. B., et al. 2020, *American Astronomical Society Meeting Abstracts #235*, Vol. *235*, 154.05.

Evans, P. A., Page, K. L., Osborne, J. P., et al. 2020, *Astrophys. J. Suppl.*, *247*(2), 54.

Farrell, S. A., Webb, N. A., Barret, D., Godet, O., & Rodrigues, J. M. 2009, *Nature*, *460*(7251), 73.

Feng, H., & Kaaret, P. 2010, April, *Astrophys. J. Lett.*, *712*(2), L169.

Fürst, F., Walton, D. J., Harrison, F. A., et al. 2016, *Astrophys. J. Lett.*, *831*(2), L14.

Fürst, F., Walton, D. J., Stern, D., et al. 2017, *ApJ*, *834*(1), 77.

Gladstone, J. C., Roberts, T. P., & Done, C. 2009, *MNRAS*, *397*(4), 1836.

Israel, G. L., Belfiore, A., Stella, L., et al. 2017, *Science*, *355*(6327), 817.

Israel, G. L., Papitto, A., Esposito, P., et al. 2017, *MNRAS*, *466*(1), L48.

Kaaret, P., Feng, H., & Roberts, T. P. 2017, *ARA&A*, *55*(1), 303.

Kovlakas, K., Zezas, A., Andrews, J. J., et al. 2020, *MNRAS*, *498*(4), 4790.

Lin, L. C.-C., Hu, C.-P., Li, K.-L., et al. 2020, *MNRAS*, *491*(4), 5682.

Makarov, D., Prugniel, P., Terekhova, N., Courtois, H., & Vauglin, I. 2014, *A&A*, *570*, A13.

Mezcua, M., Roberts, T. P., Lobanov, A. P., & Sutton, A. D. 2015, *MNRAS*, *448*(2), 1893.

Pasham, D. R., Strohmayer, T. E., & Mushotzky, R. F. 2014, *Nature*, *513*(7516), 74.

Roberts, T. P., & Warwick, R. S. 2000, *MNRAS*, *315*(1), 98.

Rodríguez Castillo, G. A., Israel, G. L., Belfiore, A., et al. 2020, *Astrophys. J.*, *895*(1), 60.

Sathyaprakash, R., Roberts, T. P., Walton, D. J., et al. 2019, *MNRAS*, *488*(1), L35.

Song, X., Walton, D. J., Lansbury, G. B., Evans, P. A., Fabian, A. C., Earnshaw, H., & Roberts, T. P. 2020, *MNRAS*, *491*(1), 1260.

Sutton, A. D., Roberts, T. P., Gladstone, J. C., & Walton, D. J. 2015, *MNRAS*, *450*(1), 787.

Sutton, A. D., Roberts, T. P., Walton, D. J., Gladstone, J. C., & Scott, A. E. 2012, *MNRAS*, *423*(2), 1154.

Swartz, D. A., Ghosh, K. K., Tennant, A. F., & Wu, K. 2004, *ApJS*, *154*(2), 519.

Tsygankov, S. S., Mushtukov, A. A., Suleimanov, V. F., & Poutanen, J. 2016, *MNRAS*, *457*(1), 1101.

Walton, D. J., Harrison, F. A., Bachetti, M., et al. 2015, *ApJ*, *799*(2), 122.

Walton, D. J., Mackenzie, A. D. A., Gully, H., Patel, N. R., Roberts, T. P., Earnshaw, H. P., & Mateos, S. 2022, *MNRAS*, *509*(2), 1587.

Walton, D. J., Roberts, T. P., Mateos, S., & Heard, V. 2011, *MNRAS*, *416*(3), 1844.

Webb, N., Cseh, D., Lenc, E., et al. 2012, *Science*, *337*(6094), 554.

Webb, N. A., Coriat, M., Traulsen, I., et al. 2020, *Astron. Astrophys.*, *641*, A136.